EUROPEAN ORGANIZATION FOR NUCLEAR RESEARCH

CERN-EP/85-05
16 January 1985

FIRST OBSERVATION OF K X-RAYS FROM $p\bar{p}$ ATOMS[+]

The ASTERIX Collaboration

S. Ahmad [1)*], C. Amsler[2)], R. Armenteros[3)], E.G. Auld[4)], D. Axen[4)], D. Bailey[3)], S. Barlag[3)], G.A. Beer[5)], J.C. Bizot[1)], M. Caria[2)**], M. Comyn[6)], W. Dahme[7)], B. Delcourt[1)], M. Doser[2)], K.D. Duch[8)], K.L. Erdman[4)], F. Feld-Dahme[7)], U. Gastaldi[3)], M. Heel[8)], R. Howard[4)], B. Howard[4)], J. Jeanjean[1)], H. Kalinowsky[8)], F. Kayser[8)], E. Klempt[8)], R. Landua[3)], G. Marshall[5)], H. Nguyen[1)], N. Prévot[1)], L. Robertson[5)], C. Sabev[9)], U. Schaefer[7)], R. Schneider[8)], O. Schreiber[8)], U. Straumann[8)], P. Truoel[2)], B. White[4)], W.R. Wodrich[7)], and M. Ziegler[8)]

ABSTRACT

K and L series X-rays have been observed from $p\bar{p}$ atoms formed in hydrogen gas at NTP in association with annihilations into neutral particles. The strong interaction shifts the energy of the 1s level by (-0.5 ± 0.3) keV. The K_α X-ray yield is $(2.6 \pm 1.3) \times 10^{-3}$ per stopped antiproton.

(Submitted to Physics Letters B)

---

1) Laboratoire de l'Accélérateur Linéaire, Orsay, France.
2) University of Zurich, Switzerland.
3) CERN, Geneva, Switzerland.
4) University of British Columbia, Vancouver, B.C., Canada.
5) University of Victoria, Victoria, B.C., Canada.
6) TRIUMF, Vancouver, B.C., Canada.
7) University of Munich, Fed. Rep. Germany.
8) University of Mainz, Fed. Rep. Germany.
9) Visitor at CERN, Geneva, Switzerland.
+ This work comprises part of the thesis (D 77) of O. Schreiber.
* Now at TRIUMF, Vancouver, B.C., Canada.
** Now at the University of Cagliari, Italy.

Antiprotonic hydrogen atoms provide a unique tool for studying the strong $p\bar{p}$ interaction at threshold. As the widths and energies of the S- and P-states are particularly sensitive to the $p\bar{p}$ interaction, the spectrum of L(nd $\rightarrow$ 2p) and K(np $\rightarrow$ 1s) X-rays emitted during the atomic cascade of $p\bar{p}$ atoms is of considerable experimental and theoretical interest.

The Dirac theory gives energies of 1.74 keV for the $L_\alpha(3 \rightarrow 2)$ and 9.37 keV for the $K_\alpha(2 \rightarrow 1)$ transition. Various theoretical models [1–5] predict the strong interaction in the atomic ground state to be repulsive and to shift and broaden the 1s level by 0.5 to 1.0 keV. The hyperfine splitting between the singlet and triplet S-states is predicted to be between 0.22 and 0.28 keV owing to the spin-dependent $N\bar{N}$ interaction [3, 4].

Two experiments have previously searched for X-ray transitions to the low-lying levels of the $p\bar{p}$ atom formed in liquid H_2 targets [6, 7]. The first observation of L X-rays was reported by an experiment using a hydrogen gas target at 4 atm [8]. The very intense flux of antiprotons from the new Low-Energy Antiproton Ring (LEAR) [9] at CERN allows a more thorough study, and three experiments [10–12] are currently attempting to measure the strong interaction effects on the X-ray spectrum of antiprotonic hydrogen.

In this letter we report the first observation of X-ray transitions to the ground state of the $p\bar{p}$ atom. The $p\bar{p}$ atoms were required to annihilate into neutral particles only, thus strongly suppressing the background from inner bremsstrahlung and from misidentified tracks of charged particles.

The experiment was performed in the North 2 beam line at LEAR with a beam momentum of 308 MeV/c and a momentum spread of $\Delta p/p = 2 \times 10^{-3}$. The average $\bar{p}$ flux was 2×10^4 antiprotons per second.

Figure 1 shows the central part of the ASTERIX detector [13]. Antiprotons from LEAR pass through scintillation counters and enter a 76 cm long, 16 cm diameter, gaseous hydrogen target (NTP). The trigger for antiprotons stopping in the target is defined by the counter telescope (T1, T2) followed by two veto counters (T3, T4). The $\bar{p}$ STOP ($= T1 \cdot T2 \cdot \overline{T3} \cdot \overline{T4}$) rate was typically 10% of the incoming flux.

A cylindrical X-ray drift chamber (XDC) [14] surrounds the hydrogen target. The XDC gas (50% argon + 50% ethane) is separated from the hydrogen target by a thin 6 μm aluminized Mylar membrane (at high voltage) which is transparent to X-rays with energies greater than 1 keV. The energy of X-rays which are absorbed in the drift chamber gas is measured on 90 signal wires (at ground voltage) running parallel to the beam axis (z axis) at a radius of 14.4 cm. The pulse height on each wire is sampled every 32 ns by flash ADCs giving information on the shape of the pulse. The drift time determines the conversion radius. The maximum drift length of 6.4 cm corresponds to a drift time of 1.4 μs. The z coordinate along the wire is determined by charge division of signals from both ends of the wires. A detailed description of the electronics has been given elsewhere [15].

Charged particles are detected also by seven cylindrical multiwire proportional chambers (MWPCs) surrounding the XDC and located in a solenoidal magnetic field. The solid angle subtended by the two innermost chambers is 75%.

A total of 6×10^5 events were recorded during six hours of beam time. The trigger required a $\bar{p}$ STOP signal, a single hit wire and no hit on adjacent wires in the XDC to select events with X-ray candidates [16], and no hit in the two inner MWPCs of the spectrometer. The MWPC veto suppresses $p\bar{p}$ annihilation with charged particles in the final state. Accepted events were read by a PDP 11/60 computer and written onto magnetic tape.

In the off-line analysis, X-ray candidates are required to have

- only one XDC wire with a pulse in the full drift-time window;
- a distinctive X-ray pulse shape, well established by X-rays from calibration sources;

- the X-ray conversion point in the region -20 cm $< z < +17$ cm (the centre of the XDC being at $z = 0$) and at a distance of more than 1.5 cm from the Mylar foil.

The first two cuts suppress events with annihilations into charged particles. Charged particles usually fire several XDC wires and can be distinguished from X-rays by their characteristically long pulse shape, whilst X-ray conversions are well isolated in space. The other cuts are explained below.

The resulting X-ray spectrum is shown in Fig. 2. The top right part of the figure shows the spectrum above 4 keV, enlarged by a factor of ~ 20. The large peak between 0.9 and 3.3 keV originates from the L series of antiprotonic hydrogen already observed by Auld et al. [8]. Entries in the region below 1 keV are due to electronic noise. The region above 4 keV shows a broad structure between 6.9 and 11.0 keV. We attribute this structure to the K series of X-rays populating the 1s state for the reasons discussed in the following.

Figure 3 shows the distribution of X-ray conversion points along the XDC axis for a) the 'low-energy' region from 0.9 to 3.3 keV and b) the 'high-energy' region from 6.9 to 11.0 keV. This distribution should agree with that of stopped antiprotons in hydrogen, which is approximately flat owing to the large width of the $\bar{p}$ range curve and which is known from events associated with charged final states. For the low-energy X-rays (L-series) the distribution is uniform with a slight increase at higher z values. For the high-energy X-rays (K series) the flat region is limited to -20 cm $< z < +17$ cm, and the distribution increases significantly towards the ends. This indicates the existence of background contamination at both ends of the XDC. The origins of this background are understood and are discussed below. To reduce the background contributions to the X-ray spectra, we select only X-rays converting within the flat region along z.

Figure 4 shows the drift-time distributions of converted X-rays in the two energy regions. The drift time measures the distance of the X-ray conversion from the anode wires. Both distributions decrease with increasing distance from the target region. This behaviour is expected from the attenuation length of X-rays coming from within the target. The two slopes are in agreement with the expected absorption distribution of the corresponding energy range.

Possible sources of background and the cuts applied to minimize them are the following:

1) *Charged particles:* Annihilations into charged particles, whether or not accompanied by neutral particles, can occur with the charged particles escaping detection. The XDC also works as a projection chamber, and tracks are found by a three-dimensional pattern recognition program. In addition, the charged particle pulse shape is very different from the X-ray pulse shape. The probability for a charged particle to be misidentified as an X-ray is less than 10^{-2}. This background occurs mainly at the ends of the XDC, where tracks almost parallel to the Mylar foil can leave the apparatus without being fully detected. The energy distribution of these particles has been studied in separate runs with charged final states. It peaks at 2–3 keV and decreases smoothly toward higher energies. The cut in z and the requirement that a conversion point must be at least 1.5 cm away from the Mylar foil removes most of this background.
2) *Inner bremsstrahlung:* X-rays due to inner bremsstrahlung are produced by $p\bar{p}$ annihilation into charged particles [17]. Since the trigger vetoes charged particles, the X-ray yield from inner bremsstrahlung is much suppressed.
3) *X-rays from other $p\bar{p}$ atoms:* Antiprotons can also stop in the counter gas, in the Mylar foil, in one of the scintillators, or in material at the end of the XDC. Antiprotons stopping in the argon/ethane gas are efficiently vetoed by software cuts because of their very large ionization. Stops in the Mylar foil or in the scintillators can induce $\bar{p}$C or $\bar{p}$O X-rays, but annihilation

products of these atoms are usually detected by the XDC. This suppression factor together with the approximately known $\bar{p}C$ X-ray yields [18] gives an estimated upper yield of 12 counts for all transitions in the energy region between 6 and 15 keV. The corresponding upper limit for $\bar{p}O$ is 4 counts. Antiprotons stopping in an aluminium ring at the end of the target can produce 7.1 keV ($7 \rightarrow 6$) and 9.5 keV ($6 \rightarrow 5$) X-rays. Their characteristic contribution is known from their conversion distribution along the XDC axis, which is strongly peaked towards the end. Figure 5 shows the X-ray spectrum produced by antiprotons stopping outside the target region. The large peak at 3 keV is due to argon fluorescence, and the peak at 7.1 keV to the $\bar{p}Al$ ($7 \rightarrow 6$) transition.

4) *Random coincidences:* A 200 nCi ^{54}Mn calibration source emitting 5.5 keV X-rays is positioned on the counter T4 at the downstream end of the XDC. Random coincidences between a $\bar{p}$ STOP signal and a source X-ray create a 5.5 keV background with a z distribution peaked near T4. Most of these X-rays are removed by the z cut. Their drift time is randomly distributed. By counting the number of X-rays in the 5.5 keV energy region arriving at drift times outside the allowed drift-time window defined by a $\bar{p}$ STOP trigger, the contribution within the drift-time window is determined to be 40 ± 6.
5) *Contamination of the target gas:* Argon and ethane diffusion or leakage through the Mylar foil can contaminate the hydrogen gas. The argon contamination was measured by mass spectroscopy to be 7 ppm. An upper limit of 3×10^{-4} for the yield per antiproton stop is estimated from known transfer rates of muons from muonic hydrogen to argon [19] and from the approximate X-ray yield from the $\bar{p}Ar$ cascade in the 'high energy' region (6.9 to 11 keV). This holds also for ethane, where the transfer rate is even smaller. The 9 keV peak observed in the $p\bar{p}$ X-ray data (Fig. 2) is not seen in the measured background X-ray spectrum (Fig. 5), so this signal cannot be due to $\bar{p}Ar$, $\bar{p}C$, $\bar{p}Al$, or $\bar{p}O$ contamination.

We conclude that the peak around 9 keV is due to the emission of K X-rays from antiprotonic hydrogen. The analysis of this energy region has to take into account several aspects of the strong interaction. Transitions to the 1s state can lead to the two hyperfine states ($^3S_1$ or $^1S_0$); isospin singlet and triplet components are assumed to be represented with equal strength. The spin and isospin dependence of the strong interaction therefore determines the shift and broadening of each of the two K lines representing transitions into one of the hyperfine states.

As these parameters are unknown and present statistics are insufficient for their complete determination, the following simple model has been used to fit the data. In the K-line region we have assumed two Gaussians with a line width fixed by the experimental resolution [$\Delta E = 1.5$ keV (FWHM) at 9.0 keV] and with a fixed distance $E(K_\beta) - E(K_\alpha) = 1.74$ keV. For the background we have assumed contributions from inner bremsstrahlung, a smooth charged-particle background, 40 random coincidences with the ^{54}Mn 5.5 keV line, and 2 $\bar{p}Al$ ($7 \rightarrow 6$ and $6 \rightarrow 5$) lines at 7.1 keV and 9.5 keV.

The energy calibration and the energy resolution of the XDC were determined with X-ray sources (^{54}Mn: 5.5 keV and escape peak, ^{60}Co: 14.4 keV), the 1.74 keV L_α line from the $p\bar{p}$ atom, and the 3.0 keV argon fluorescence line. The resolution is $\sigma(E) = 0.09 \sqrt{5.5\ E}$ keV. The detection efficiency was determined using a Monte Carlo program based on the stop distribution of antiprotons in the target as determined from charged track vertices from separate runs. The events were analysed with the same program and identical software cuts as those for the real data in order to give the detection efficiency as a function of energy (Fig. 6a).

The spectrum has 694 entries in the energy region between 6 and 16 keV. The fit gives 127 entries for the K_α line and 108 entries for the K_β line. The average background from charged particles is 15 entries per 0.33 keV bin. For the $\bar{p}Al$ ($7 \rightarrow 6$) line at 7.1 keV it finds 64 entries, and

an upper limit of 20 entries for the $\bar{p}$Al (6 → 5) line at 9.5 keV. The fitting program finds no contribution from X-rays with the energy distribution of inner bremsstrahlung. Figure 6b shows the spectrum corrected for the detection efficiency after subtraction of the charged-particle background.

The best fit has χ^2/d.f. = 1.2 and yields a K_α X-ray energy of 8.9 ± 0.3 keV, corresponding to a shift of the 1s level $\Delta E_{1s} = -0.5 \pm 0.3$ keV. The use of other models to fit the data can result in a different shift. The relative yield of the K_α line compared with all K transitions is $Y(K_\alpha)/[Y(K_\alpha) + Y(K_\beta)] = 0.4 \pm 0.1$.

The relative K to L X-ray yield depends on the unknown branching ratio for annihilation into neutral particles from atomic p states. For example, if this branching ratio were bigger in the p-wave, a veto on charged particles would prefer annihilation from the P-states and hence suppress K X-ray emission. Assuming the branching ratios from s and p states to be equal, the relative yield is $Y(K_\alpha)/Y(L_{tot}) = (2 \pm 1) \times 10^{-2}$.

From X-ray spectra taken in coincidence with annihilations into two or more prongs, the absolute yield for the total L-line yield has been determined to be $Y(L_{tot}) = 0.13 \pm 0.02$ per antiproton stop [20]. Therefore, under the above assumptions, the absolute K_α yield is estimated to be $(2.6 \pm 1.3) \times 10^{-3}$.

Although these results are compatible with most theoretical predictions, they must be considered as being only a first step towards a more complete picture of the complex structure of the $p\bar{p}$ atom ground state. Further analysis of data taken in 1984 with much higher statistics will allow us to look for coincidences between L and K_α X-rays, thus giving us the possibility to see the isolated K_α peak in the coincidence spectrum. Coincidences between K transitions and subsequent annihilation into two charged pions only identify the $^3S_1$ level and can be used to identify the hyperfine splitting of the ground state.

Acknowledgements

We are indebted to the LEAR staff for their strong support. This work was supported by the Deutsches Bundesministerium für Forschung und Technologie, by the Institut National de Physique Nucléaire et de Physique des Particules, in part by the Schweizer Nationalfond, and by the Natural Sciences and Engineering Research Council of Canada.

REFERENCES

[1] B.O. Kerbikov, Proc. 5th European Symposium on Nucleon–Antinucleon Interactions, Bressanone, 1980 (CLEUP, Padua, 1980), p. 423. [Reference to earlier work can be found herein.]

[2] W.B. Kaufmann, Phys. Rev. **19C** (1979) 440.

[3] J.M. Richard and M.E. Sainio, Phys. Lett. **110B** (1982) 349.

[4] A.M. Green and S. Wycech, Nucl. Phys. **A377** (1982) 441.

[5] M.A. Alberg et al., Phys. Rev. **D27** (1983) 536.

[6] R.E. Welsh, Proc. 7th Int. Conf. on High-Energy Physics and Nuclear Structure, Zurich, 1977, ed. M.P. Locher (Birkhäuser Verlag, Basle, 1977), p. 95.

[7] M. Iżycki et al., Z. Phys. **A297** (1980) 1.

[8] E. Auld et al., Phys. Lett. **77B** (1978) 454.

[9] P. Lefèvre et al., Proc. 11th Int. Conf. on High-Energy Accelerators, Geneva, 1980 (Birkhäuser Verlag, Basle, 1980), p. 819.

[10] S. Ahmad et al. (ASTERIX Collaboration), Proc. Workshop on Physics at LEAR with Low-Energy Cooled Antiprotons, Erice, 1982, eds. U. Gastaldi and R. Klapisch (Plenum Press, New York, 1984), p. 109.

[11] J. Davies et al., same Proceedings, p. 143.

[12] D. Gotta, same Proceedings, p. 165.

[13] S. Ahmad et al. (ASTERIX Collaboration), The ASTERIX spectrometer, to be submitted to Nuclear Instruments and Methods.

[14] U. Gastaldi, M. Heel, H. Kalinowsky, E. Klempt, R. Landua, R. Schneider, O. Schreiber, R.W. Wodrich and M. Ziegler, Construction and operation of the spiral projection chamber, to be submitted to Nuclear Instruments and Methods.

U. Gastaldi, Nucl. Instrum. Methods **157** (1978) 441.

U. Gastaldi, Nucl. Instrum. Methods **188** (1981) 459.

[15] M. Calvetti et al., Nucl. Instrum. Methods **176** (1980) 255.

[16] H. Kalinowsky, The ASTERIX trigger system, to be submitted to Nuclear Instruments and Methods.

H. Lenz, Diplomarbeit, 1982, Universität Mainz (unpublished).

[17] R. Rückl and Č. Zupančič, submitted to Physics Letters B.

[18] R.E. Welsh, private communication.

[19] E. Iacopini et al. , Nuovo Cimento **67A** (1982) 201.

[20] S. Ahmad et al. (ASTERIX Collaboration), First observation of K X-rays from antiprotonic hydrogen atoms, to be published in Proc. 7th European Symp. on Proton–Antiproton Interactions, Durham, 1984.

Figure captions

Fig. 1 : H_2 target (16 cm diameter), XDC central detector (Spiral Projection Chamber), and T1, T2, T3, and T4 plastic scintillators.

Fig. 2 : X-ray energy spectrum after all cuts. The smooth curve is the fitted spectrum.

Fig. 3 : X-ray conversion point distribution along the XDC axis (z):
a) for low-energy X-rays (E = 0.9–3.3 keV);
b) for high-energy X-rays (E = 6.9–11.0 keV).
The accepted fiducial region is between $-20\ \text{cm} \lesssim z \lesssim +17\ \text{cm}$.

Fig. 4 : X-ray drift-time distribution:
a) for low-energy X-rays (E = 0.9–3.3 keV);
b) for high-energy X-rays (E = 6.9–11.0 keV).
The accepted fiducial drift-time is $0.2 \lesssim t \lesssim 1.1\ \mu s$.

Fig. 5 : X-ray energy spectrum associated with antiprotons stopping outside the target region.

Fig. 6a : Calculated X-ray detection efficiency.

Fig. 6b : X-ray energy spectrum after subtraction of the charged-particle background and correction for the detection efficiency.

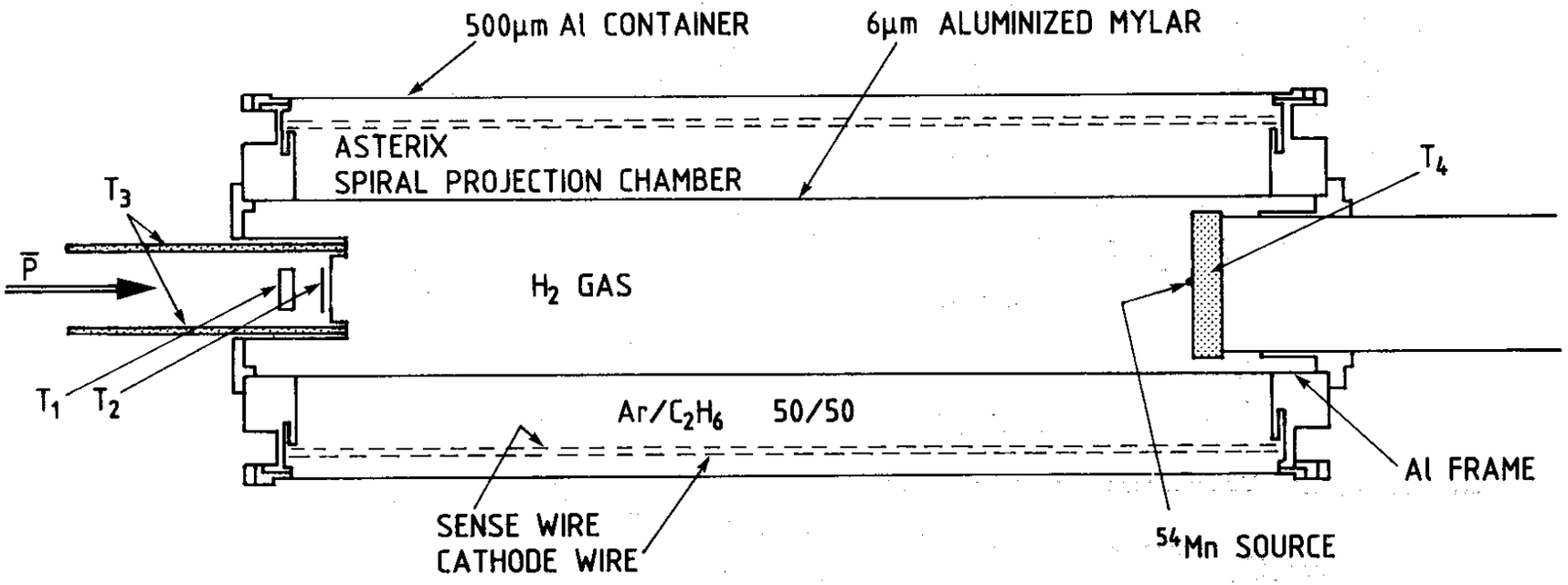
500µm Al CONTAINER
6µm ALUMINIZED MYLAR
ASTERIX
SPIRAL PROJECTION CHAMBER
T3
T4
P̄
H2 GAS
T1
T2
Ar/C2H6 50/50
Al FRAME
SENSE WIRE
CATHODE WIRE
54Mn SOURCE

Fig. 1

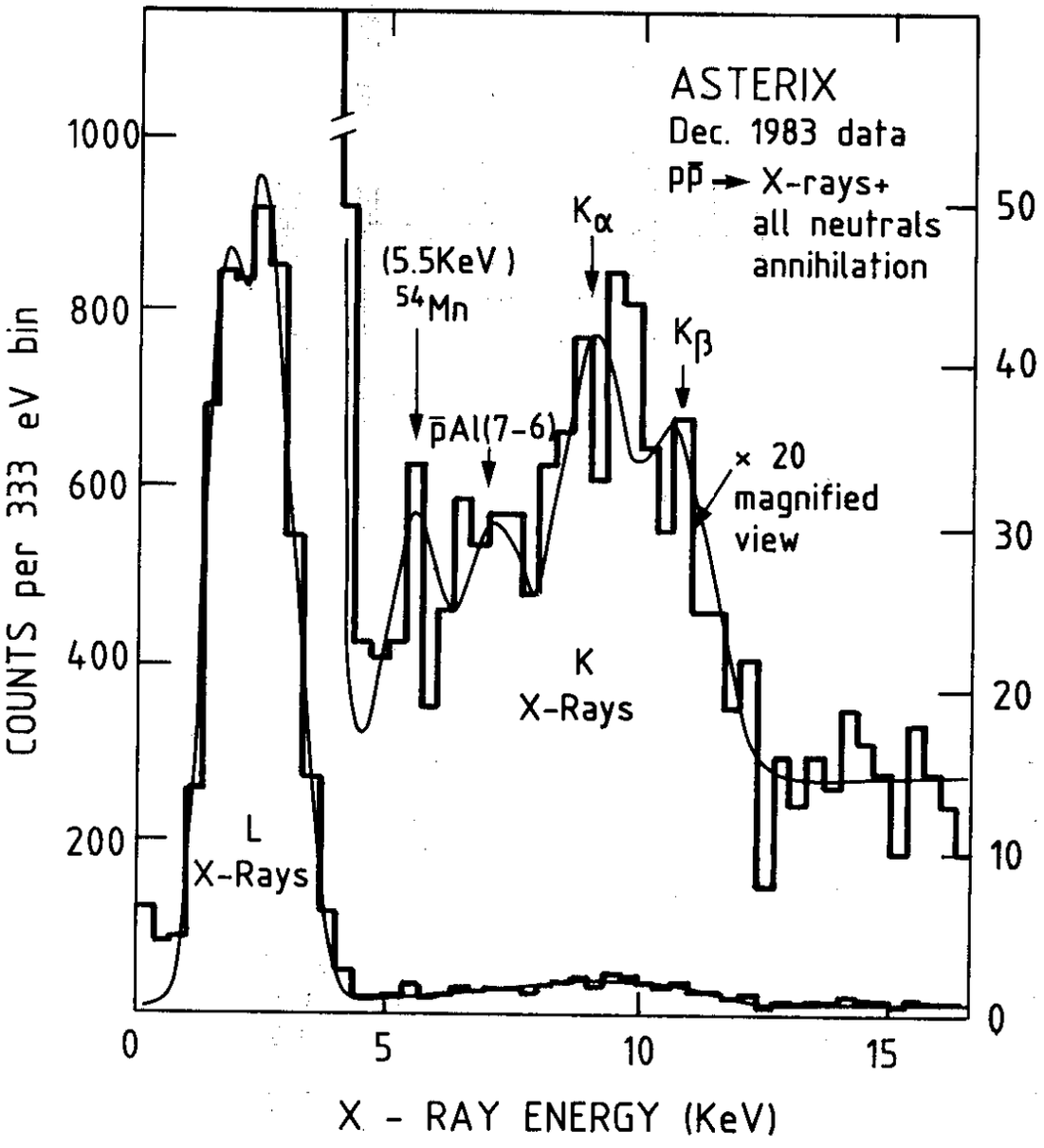
ASTERIX
Dec. 1983 data
$p\bar{p}$ → X-rays+
all neutrals
annihilation
K_α
K_β
(5.5KeV)
^{54}Mn
$\bar{p}$Al(7-6)
× 20
magnified
view
K
X-Rays
L
X-Rays
COUNTS per 333 eV bin
X - RAY ENERGY (KeV)
1000
800
600
400
200
0
5
10
15
50
40
30
20
10
0

Fig. 2

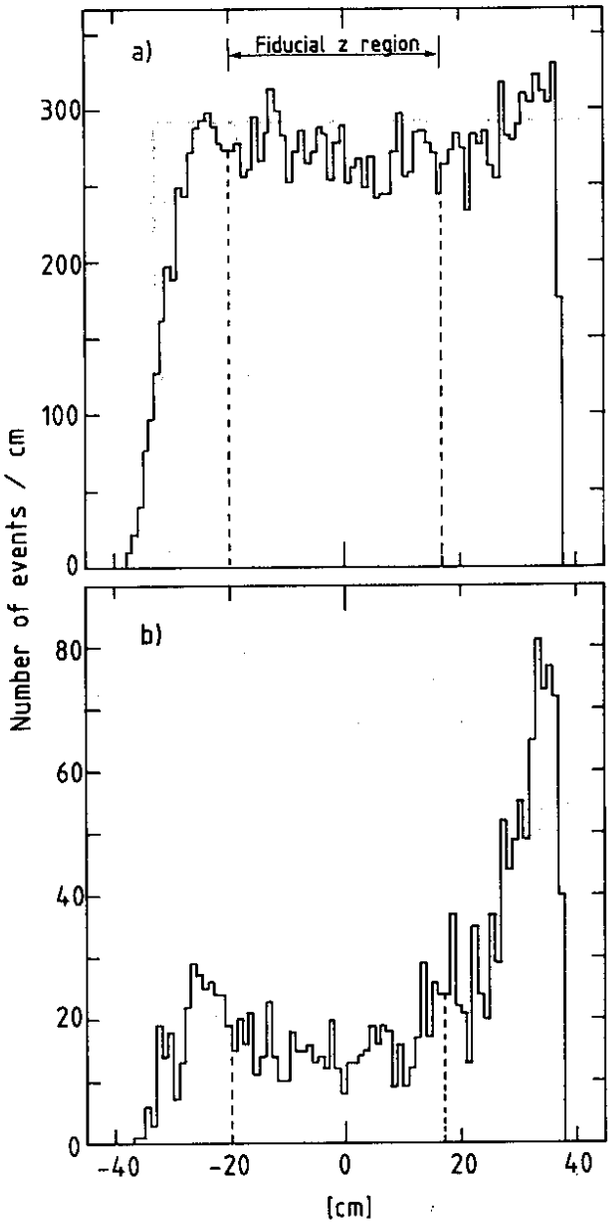
a)
Fiducial z region
300
200
100
0
b)
80
60
40
20
0
-40
-20
0
20
40
[cm]
Number of events / cm

Fig. 3

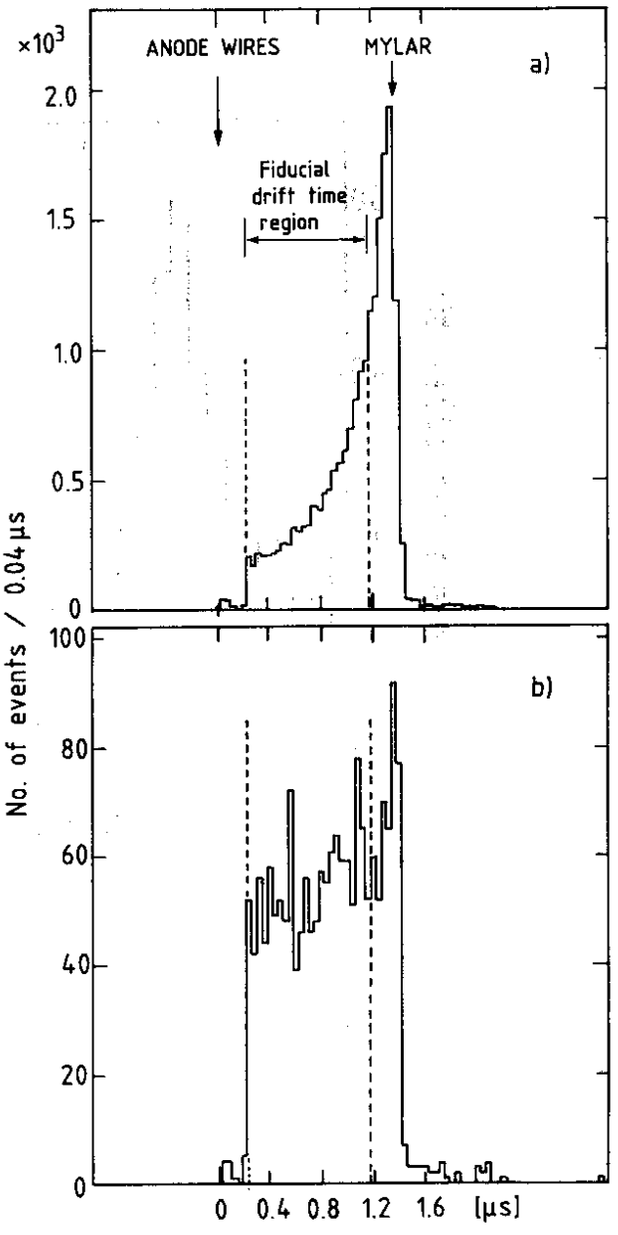
×10³
ANODE WIRES
MYLAR
a)
2.0
1.5
1.0
0.5
0
Fiducial
drift time
region
b)
100
80
60
40
20
0
0
0.4
0.8
1.2
1.6
[μs]
No. of events / 0.04 μs

Fig. 4

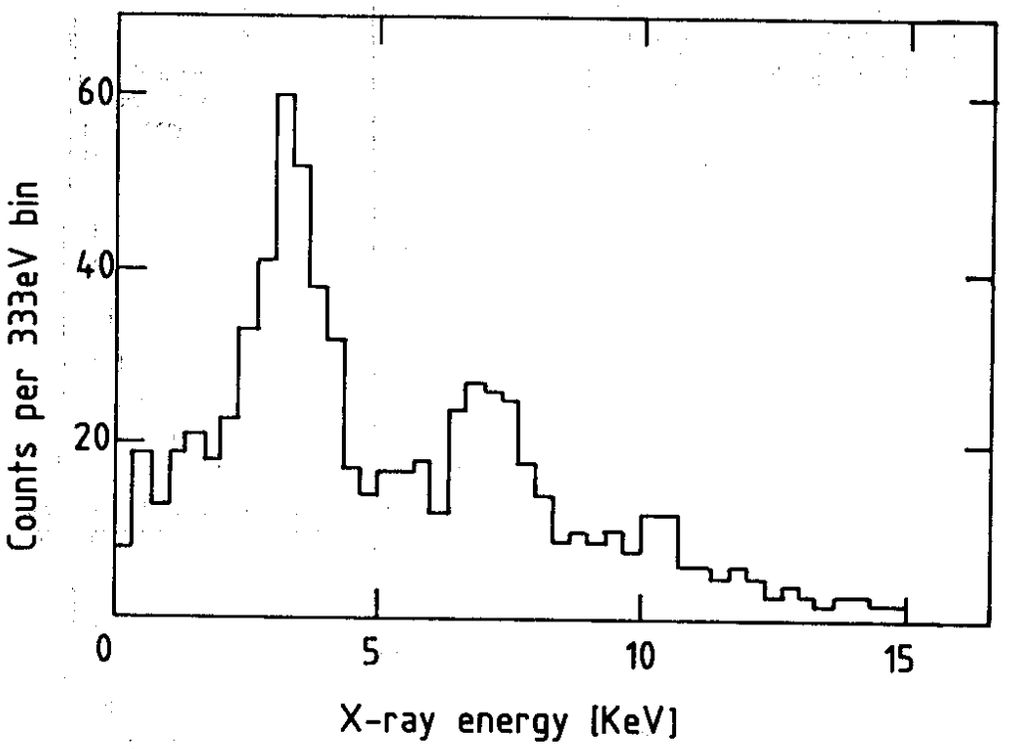

Fig. 5

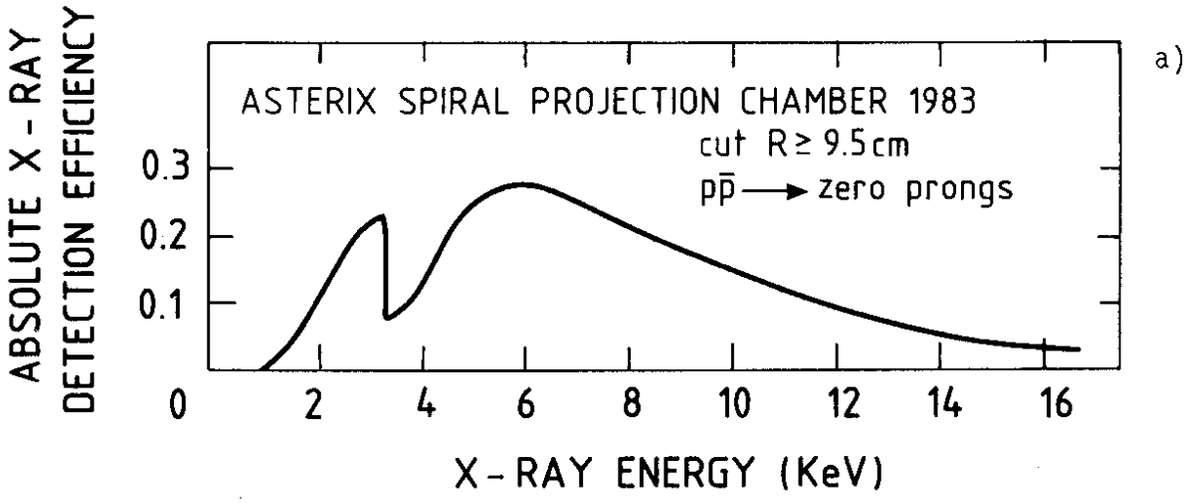
a)
ABSOLUTE X-RAY DETECTION EFFICIENCY
ASTERIX SPIRAL PROJECTION CHAMBER 1983
cut R ≥ 9.5cm
pp̄ → zero prongs
0.3
0.2
0.1
0
2
4
6
8
10
12
14
16
X-RAY ENERGY (KeV)

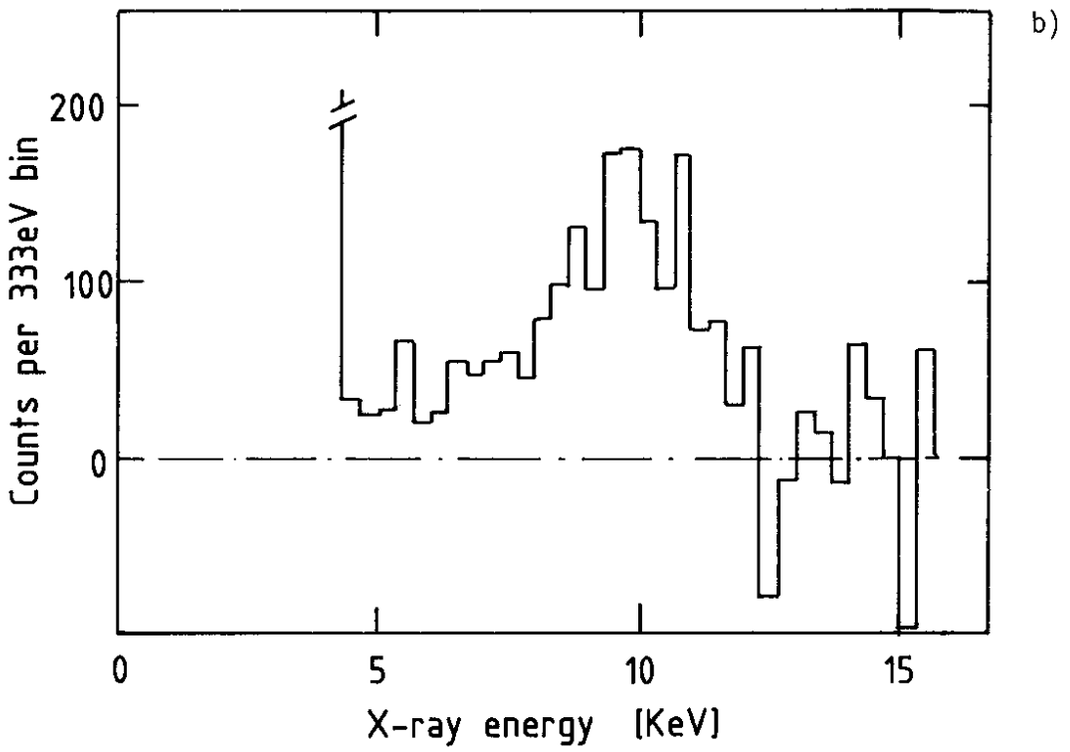
b)
Counts per 333eV bin
200
100
0
0
5
10
15
X-ray energy [KeV]

Fig. 6